Available online at www.sciencedirect.com
SCIENCE DIRECT®
ELSEVIER
International Journal of Solids and Structures 43 (2006) 1239–1252
INTERNATIONAL JOURNAL OF SOLIDS and STRUCTURES
www.elsevier.com/locate/ijsolstr

Anti-plane analysis of a functionally graded strip with multiple cracks

A.R. Fotuhi [a], S.J. Fariborz [a,b,*]

[a] *Department of Mechanical Engineering, Amirkabir University of Technology (Tehran Polytechnic), 424, Hafez Avenue, Tehran 158754413, Iran*
[b] *Faculty of Engineering, Persian Gulf University, Bushehr, Iran*

Received 9 November 2004; received in revised form 24 March 2005
Available online 23 May 2005

Abstract

The stress fields are obtained for a functionally graded strip containing a Volterra screw dislocation. The elastic shear modulus of the medium is considered to vary exponentially. The stress components exhibit Cauchy as well as logarithmic singularities at the dislocation location. The dislocation solution is utilized to formulate integral equations for the strip weakened by multiple smooth cracks under anti-plane deformation. Several examples are solved and stress intensity factors are obtained.

Keywords: Anti-plane; Strip; Screw dislocation; Multiple cracks; Functionally graded material

1. Introduction

The advent of materials with continuously varying volume fractions, the so-called functionally graded materials (FGMs), and their technological potential have stimulated a fair amount of research in this area. In principle, by controlling the material gradation during the manufacturing process of a mechanical component fabricated from FGMs, the desired thermomechanical response may be attained. From the mathematical point of view, the analysis of FGMs requires the solution of differential equations with variable rather than constant coefficients. In the mixed boundary value problems, arising in the fracture of FGMs,

* Corresponding author. Tel.: +98 21 6454 3460; fax: +98 21 641 9736.
E-mail address: sjfariborz@yahoo.com (S.J. Fariborz).

0020-7683/$ - see front matter © 2005 Elsevier Ltd. All rights reserved.
doi:10.1016/j.ijsolstr.2005.03.066

it is customary to approximate the constitutive law to render the final differential equations with constant coefficients.

Various crack problems in FGMs, under in-plane and anti-plane deformations, have been tackled recently. A brief review of articles concerning cracks under anti-plane shear are mentioned below. Erdogan (1985) solved the problem of a crack perpendicular to the direction of interface of two half-planes of different FGMs. Two bonded isotropic half-planes with non-homogeneous interfacial zone weakened by a crack in each region, where cracks were perpendicular to the direction of interface, was analyzed by Erdogan et al. (1991). Crack at the interface of a FGM and a rigid half-plane was analyzed by Erdogan and Ozturk (1992). In another paper Ozturk and Erdogan (1993) obtained stress intensity factor and strain energy release rate for an interface crack between an elastic half-plane and a non-homogenous strip whose other edge was bonded to another elastic half-plane. The application of hypersingular integral equations to crack problems in non-homogeneous medium was studied by Chan et al. (2001). Huang et al. (2002) considered the coating of a half-plane with FGM. The coating zone contained a crack, and was divided into sublayers with linearly varying material property. The stress analysis in a non-homogeneous interfacial zone between two dissimilar elastic solids was accomplished by Wang et al. (2003a). The stress intensity factor in a FGM strip containing crack parallel to the edge was obtained by Wang et al. (2003b).

In the present article, we employ the distributed dislocation technique to analyze multiple curved cracks in a FGM strip under anti-plane shear. The shear modulus of material is represented by an exponential function. The technique necessities the solution of screw Volterra dislocation in the region. The complex Fourier transform is employed and two solutions in series and integral forms are obtained for stress fields. The solutions are then used to obtain singular integral equations for the dislocation density on the surface of multiple cracks. These equations are solved numerically and the solutions are employed to determine stress intensity factors for cracks with different configurations and arrangements.

2. Strip with screw dislocation

We consider a strip with thickness h made up of FGM, where the elastic shear modulus μ varies continuously in the thickness direction, Fig. 1. Under conditions of anti-plane deformation the only component of the displacement vector is the out-of-plane component $w(x, y)$. Consequently, the constitutive relationships read as

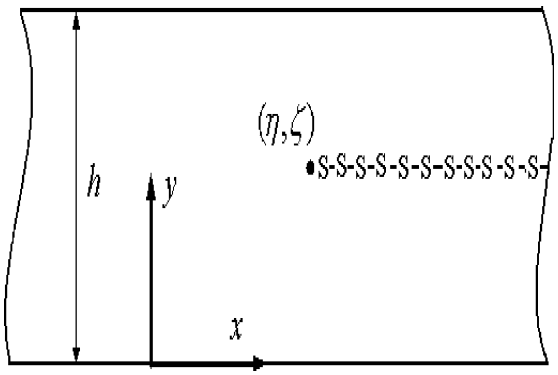

Fig. 1. Strip weakened by a screw dislocation.

$$\tau_{xz} = \mu(y)\frac{\partial w}{\partial x}$$
$$\tau_{yz} = \mu(y)\frac{\partial w}{\partial y} \tag{1}$$

Utilizing Eq. (1) the equilibrium equation in terms of displacement may be written as

$$\frac{\partial^2 w}{\partial x^2} + \frac{\partial^2 w}{\partial y^2} + \frac{\mu'(y)}{\mu(y)}\frac{\partial w}{\partial y} = 0 \tag{2}$$

Eq. (2) is solved by means of the complex Fourier transform defined by

$$F(s) = \int_{-\infty}^{\infty} f(x)\mathrm{e}^{-\mathrm{i}sx}\,\mathrm{d}x \tag{3}$$

where $\mathrm{i} = \sqrt{-1}$. The inversion of (3) is

$$f(x) = \frac{1}{2\pi}\int_{-\infty}^{\infty} F(s)\mathrm{e}^{\mathrm{i}sx}\,\mathrm{d}s \tag{4}$$

Applying (3) to Eq. (2) with the aid of integrations by parts and in conjunction with the property of decaying behavior of displacement and stress components as $|x| \to \infty$ leads to

$$\frac{\mathrm{d}^2 W}{\mathrm{d}y^2} + \frac{\mu'(y)}{\mu(y)}\frac{\mathrm{d}W}{\mathrm{d}y} - s^2 W = 0 \tag{5}$$

In Eq. (5), $W(s,y)$ is the Fourier transform of displacement field. To facilitate the solution of the above differential equation, the elastic shear modulus of FGM is considered as

$$\mu(y) = \mu_0 \mathrm{e}^{2\lambda y} \tag{6}$$

where μ_0 and λ are material constants. It is noteworthy to mention that by applying a suitable transformation to Eq. (5) a wider class of FGMs i.e., FGMs with three material constants, which renders a constant coefficient differential equation for transformed displacement may be achieved (Erdogan and Ozturk, 1992). Substituting (6) into (5) and solving the resultant equation, we arrive at

$$W(s,y) = A(s)\mathrm{e}^{(\beta-\lambda)y} + B(s)\mathrm{e}^{-(\beta+\lambda)y} \tag{7}$$

where $\beta = \sqrt{\lambda^2 + s^2}$ and $A(s)$ and $B(s)$ are unknown. The traction-free condition on the strip boundaries implies that

$$\tau_{yz}(x,0) = 0$$
$$\tau_{yz}(x,h) = 0, \quad |x| < \infty \tag{8}$$

Let a Volterra type screw dislocation with Bergers vector b_z be situated in the strip at the point with coordinates (η,ζ). The dislocation line is depicted in Fig. 1. The conditions representing the dislocation are (Faal et al., 2004)

$$w(x,\zeta^-) - w(x,\zeta^+) = b_z H(x-\eta)$$
$$\tau_{yz}(x,\zeta^-) = \tau_{yz}(x,\zeta^+), \quad |x| < \infty \tag{9}$$

where $H(x)$ is the Heaviside-step function. The first Eq. (9) enforces the multivaluedness of displacement while the second implies the continuity of traction along the dislocation line. The Fourier transform of (8) and (9) by virtue of (3) results in

$$\begin{aligned}
&\frac{\mathrm{d}W}{\mathrm{d}y}(s,0) = 0\\
&\frac{\mathrm{d}W}{\mathrm{d}y}(s,h) = 0\\
&W(s,\zeta^-) - W(s,\zeta^+) = b_z \mathrm{e}^{-\mathrm{i}s\eta}\left(\pi\delta(s) - \frac{\mathrm{i}}{s}\right)\\
&\frac{\mathrm{d}W}{\mathrm{d}y}(s,\zeta^-) - \frac{\mathrm{d}W}{\mathrm{d}y}(s,\zeta^+) = 0
\end{aligned} \tag{10}$$

where $\delta(s)$ is the Dirac delta function. Application of conditions (10) to Eq. (7) gives the unknown coefficients

$$\begin{aligned}
A(s) &= \frac{(\beta+\lambda)}{2\beta\sinh(\beta h)}\mathrm{e}^{-\mathrm{i}s\eta}\left(\pi\delta(s) - \frac{\mathrm{i}}{s}\right)b_z \times \begin{cases} \mathrm{e}^{\beta\zeta}\sinh(\beta(h-\zeta)), & 0 \leqslant y \leqslant \zeta \\ -\mathrm{e}^{-\beta(h-\zeta)}\sinh(\beta\zeta), & \zeta \leqslant y \leqslant h \end{cases}\\
B(s) &= \frac{(\beta-\lambda)}{2\beta\sinh(\beta h)}\mathrm{e}^{-\mathrm{i}s\eta}\left(\pi\delta(s) - \frac{\mathrm{i}}{s}\right)b_z \times \begin{cases} \mathrm{e}^{-\beta\zeta}\sinh(\beta(h-\zeta)), & 0 \leqslant y \leqslant \zeta \\ -\mathrm{e}^{\beta(h-\zeta)}\sinh(\beta\zeta), & \zeta \leqslant y \leqslant h \end{cases}
\end{aligned} \tag{11}$$

Substituting (11) into (7) and applying the Fourier transform inversion formula (4) yields the displacement field in the strip

$$\begin{aligned}
w(x,y) &= \frac{b_z\mathrm{e}^{\lambda\zeta}}{2}\frac{\sinh(\lambda(h-\zeta))}{\sinh(\lambda h)}\\
&\quad - \frac{\mathrm{i}b_z\mathrm{e}^{-\lambda(y-\zeta)}}{2\pi}\int_{-\infty}^{\infty}\frac{[\beta\cosh(\beta y) + \lambda\sinh(\beta y)]\sinh(\beta(h-\zeta))}{s\beta\sinh(\beta h)}\mathrm{e}^{\mathrm{i}s(x-\eta)}\,\mathrm{d}s, \quad 0 \leqslant y \leqslant \zeta\\
w(x,y) &= -\frac{b_z\mathrm{e}^{-\lambda(h-\zeta)}}{2}\frac{\sinh(\lambda\zeta)}{\sinh(\lambda h)}\\
&\quad + \frac{\mathrm{i}b_z\mathrm{e}^{-\lambda(y-\zeta)}}{2\pi}\int_{-\infty}^{\infty}\frac{[\beta\cosh(\beta(y-h)) + \lambda\sinh(\beta(y-h))]\sinh(\beta\zeta)}{s\beta\sinh(\beta h)}\mathrm{e}^{\mathrm{i}s(x-\eta)}\,\mathrm{d}s, \quad \zeta \leqslant y \leqslant h
\end{aligned} \tag{12}$$

The first terms on the right side of (12) are constant and represent the rigid body motion of strip. Furthermore, it is elementary to show that Eq. (12) satisfy the first condition (9). The stress components in view of (1) and (12) may be expressed as

$$\begin{aligned}
\tau_{yz} &= -\frac{\mathrm{i}b_z\mu_0\mathrm{e}^{\lambda(y+\zeta)}}{2\pi}\int_{-\infty}^{\infty}\frac{\sinh(\beta y)\sinh(\beta(h-\zeta))}{\beta\sinh(\beta h)}s\mathrm{e}^{\mathrm{i}s(x-\eta)}\,\mathrm{d}s, \quad 0 \leqslant y \leqslant \zeta\\
\tau_{yz} &= \frac{\mathrm{i}b_z\mu_0\mathrm{e}^{\lambda(y+\zeta)}}{2\pi}\int_{-\infty}^{\infty}\frac{\sinh(\beta(y-h))\sinh(\beta\zeta)}{\beta\sinh(\beta h)}s\mathrm{e}^{\mathrm{i}s(x-\eta)}\,\mathrm{d}s, \quad \zeta \leqslant y \leqslant h\\
\tau_{xz} &= \frac{b_z\mu_0\mathrm{e}^{\lambda(y+\zeta)}}{2\pi}\int_{-\infty}^{\infty}\frac{[\beta\cosh(\beta y) + \lambda\sinh(\beta y)]\sinh(\beta(h-\zeta))}{\beta\sinh(\beta h)}\mathrm{e}^{\mathrm{i}s(x-\eta)}\,\mathrm{d}s, \quad 0 \leqslant y \leqslant \zeta\\
\tau_{xz} &= -\frac{b_z\mu_0\mathrm{e}^{\lambda(y+\zeta)}}{2\pi}\int_{-\infty}^{\infty}\frac{[\beta\cosh(\beta(y-h)) + \lambda\sinh(\beta(y-h))]\sinh(\beta\zeta)}{\beta\sinh(\beta h)}\mathrm{e}^{\mathrm{i}s(x-\eta)}\,\mathrm{d}s, \quad \zeta \leqslant y \leqslant h
\end{aligned} \tag{13}$$

The integrals in (13) can be evaluated with the aid of contour integration and the residue theorem. The integrands have simple poles occurring at $s_n = \pm\mathrm{i}\sqrt{(\frac{n\pi}{h})^2 + \lambda^2}$, $n = 1, 2, \ldots$ whereas $s = \pm\lambda\mathrm{i}$ are regular points. To carry out the contour integration, we require that the integrands vanish as $|\, s \,| \to \infty$. Conse-

quently, for $x \geqslant \eta$, the contour of integration consists of the first and second quadrants of the complex s-plane, while for $x \leqslant \eta$, the contour engulfs the third and fourth quadrants. Utilizing the residue theorem leads to stress fields in the entire region

$$\begin{aligned}
\tau_{yz} &= \operatorname{sgn}(x-\eta)\frac{b_z\mu_0 e^{\lambda(y+\zeta)}}{2h}\sum_{n=1}^{\infty}\left[\cos\left(\frac{n\pi(y-\zeta)}{h}\right)-\cos\left(\frac{n\pi(y+\zeta)}{h}\right)\right]e^{-|x-\eta|\sqrt{(\frac{n\pi}{h})^2+\lambda^2}} \\
\tau_{xz} &= \frac{b_z\mu_0 e^{\lambda(y+\zeta)}}{2h}\sum_{n=1}^{\infty}\frac{1}{\sqrt{(\frac{n\pi}{h})^2+\lambda^2}}\left[-\frac{n\pi}{h}\left[\sin\left(\frac{n\pi(y-\zeta)}{h}\right)-\sin\left(\frac{n\pi(y+\zeta)}{h}\right)\right]\right. \\
&\quad \left.+\lambda\left[\cos\left(\frac{n\pi(y-\zeta)}{h}\right)-\cos\left(\frac{n\pi(y+\zeta)}{h}\right)\right]\right]e^{-|x-\eta|\sqrt{\left(\frac{n\pi}{h}\right)^2+\lambda^2}}
\end{aligned} \tag{14}$$

where $\operatorname{sgn}(x)$ is the sign function. For small values of $|x-\eta|$ the series solutions (14) converge slowly and a large number of terms are required to obtain accurate results. To circumvent this difficulty the integrations in (13) should be performed differently. This task is taken up by splitting the integrals in (13) into odd and even parts with respect to the parameter s and the stress fields are written as

$$\begin{aligned}
\tau_{yz} &= \frac{b_z\mu_0 e^{\lambda(y+\zeta)}}{\pi}\int_0^{\infty}\frac{\sinh(\beta y)\sinh(\beta(h-\zeta))}{\beta\sinh(\beta h)}s\sin[s(x-\eta)]\,ds, \quad 0 \leqslant y \leqslant \zeta \\
\tau_{yz} &= -\frac{b_z\mu_0 e^{\lambda(y+\zeta)}}{\pi}\int_0^{\infty}\frac{\sinh(\beta(y-h))\sinh(\beta\zeta)}{\beta\sinh(\beta h)}s\sin[s(x-\eta)]\,ds, \quad \zeta \leqslant y \leqslant h \\
\tau_{xz} &= \frac{b_z\mu_0 e^{\lambda(y+\zeta)}}{\pi}\int_0^{\infty}\frac{[\beta\cosh(\beta y)+\lambda\sinh(\beta y)]\sinh(\beta(h-\zeta))}{\beta\sinh(\beta h)}\cos[s(x-\eta)]\,ds, \quad 0 \leqslant y \leqslant \zeta \\
\tau_{xz} &= -\frac{b_z\mu_0 e^{\lambda(y+\zeta)}}{\pi}\int_0^{\infty}\frac{[\beta\cosh(\beta(y-h))+\lambda\sinh(\beta(y-h))]\sinh(\beta\zeta)}{\beta\sinh(\beta h)}\cos[s(x-\eta)]\,ds, \quad \zeta \leqslant y \leqslant h
\end{aligned} \tag{15}$$

In order to specify the singular behavior of the stress components, the asymptotic behavior of the integrands in (15) should be examined. Since the integrands are continuous functions of s and also finite at $s=0$, the singularity must occur as s tends to infinity. By virtue of the following identities:

$$\begin{aligned}
\int_0^{\infty} e^{sy}\sin(sx)\,ds &= \frac{x}{x^2+y^2}, \quad y<0 \\
\int_0^{\infty} e^{sy}\cos(sx)\,ds &= -\frac{y}{x^2+y^2}, \quad y<0
\end{aligned} \tag{16}$$

Eq. (15) may be recast to more appropriate forms

$$\begin{aligned}
\tau_{yz} &= \frac{b_z\mu_0 e^{\lambda(y+\zeta)}}{2\pi}\left[\frac{x-\eta}{r^2}+\int_0^{\infty}\left[\frac{2\sinh(\beta y)\sinh(\beta(h-\zeta))}{\beta\sinh(\beta h)}s-e^{s(y-\zeta)}\right]\sin(s(x-\eta))\,ds\right], \quad 0 \leqslant y \leqslant \zeta \\
\tau_{yz} &= -\frac{b_z\mu_0 e^{\lambda(y+\zeta)}}{2\pi}\left[\frac{x-\eta}{r^2}+\int_0^{\infty}\left[\frac{2\sinh(\beta(y-h))\sinh(\beta\zeta)}{\beta\sinh(\beta h)}s-e^{-s(y-\zeta)}\right]\sin(s(x-\eta))\,ds\right], \quad \zeta \leqslant y \leqslant h
\end{aligned}$$

$$\tau_{xz}=\frac{b_z\mu_0 e^{\lambda(y+\zeta)}}{2\pi}\left[-\frac{y-\zeta}{r^2}+\int_0^\infty\left[\frac{2\cosh(\beta y)\sinh(\beta(h-\zeta))}{\sinh(\beta h)}-e^{s(y-\zeta)}\right]\cos(s(x-\eta))\,ds\right.$$
$$+2\lambda\int_0^M\frac{\sinh(\beta y)\sinh(\beta(h-\zeta))}{\beta\sinh(\beta h)}\cos(s(x-\eta))\,ds$$
$$\left.+\lambda\int_M^\infty\left[\frac{2\sinh(\beta y)\sinh(\beta(h-\zeta))}{\beta\sinh(\beta h)}-\frac{1}{s}e^{s(y-\zeta)}\right]\cos(s(x-\eta))\,ds+\lambda\int_M^\infty\frac{1}{s}e^{s(y-\zeta)}\cos(s(x-\eta))\,ds\right],$$
$$0\leqslant y\leqslant\zeta$$

$$\tau_{xz}=-\frac{b_z\mu_0 e^{\lambda(y+\zeta)}}{2\pi}\left[\frac{y-\zeta}{r^2}+\int_0^\infty\left[\frac{2\cosh(\beta(y-h))\sinh(\beta\zeta)}{\sinh(\beta h)}-e^{-s(y-\zeta)}\right]\cos(s(x-\eta))\,ds\right.$$
$$+2\lambda\int_0^M\frac{\sinh(\beta(y-h))\sinh(\beta\zeta)}{\beta\sinh(\beta h)}\cos(s(x-\eta))\,ds$$
$$+\lambda\int_M^\infty\left[\frac{2\sinh(\beta(y-h))\sinh(\beta\zeta)}{\beta\sinh(\beta h)}-\frac{1}{s}e^{-s(y-\zeta)}\right]\cos(s(x-\eta))\,ds$$
$$\left.+\lambda\int_M^\infty\frac{1}{s}e^{-s(y-\zeta)}\cos(s(x-\eta))\,ds\right],\quad\zeta\leqslant y\leqslant h \tag{17}$$

where $r^2=(x-\eta)^2+(y-\zeta)^2$ is the distance from dislocation location and $M>0$ is an arbitrary constant which must be chosen such that it does not cause computational difficulty. The last integral in stress component τ_{xz} is the Exponential Integral (Ei) defined as (Abramowitz and Stegun, 1965).

$$\int_M^\infty\frac{\cos[s(x-\eta)]}{s}e^{-s(y-\zeta)}\,ds=-Re[\mathrm{Ei}[(-(y-\zeta)+i(x-\eta))M]]$$
$$=-\gamma_0-\log(M)-\log(r)-\sum_{k=1}^{\infty}\sum_{j=0}^{[\frac{k}{2}]}\frac{(-1)^j M^k(y-\zeta)^{k-2j}(x-\eta)^{2j}}{k(2j)!(k-2j)!},\quad y\geqslant\zeta \tag{18}$$

In Eq. (18), γ_0 is the Euler's constant, $Re[z]$ stands for the real part of z and $[\frac{k}{2}]$ is the largest integer $\leqslant\frac{k}{2}$. For the fast convergence of the series the value of M is taken less than unity. Eqs. (17) and (18) reveal that stress fields exhibit Cauchy as well as logarithmic singularity at the dislocation position. Moreover, the integrands in (17) decay sufficiently rapidly as $s\to\infty$, which makes the integrals susceptible to numerical evaluation.

3. Crack formulation

The dislocation solutions accomplished in the preceding section may be employed to analyze strip with several arbitrarily oriented cracks. The stress components caused by a screw dislocation located at (η,ζ) with dislocation line parallel to the x-axis may be written as

$$\tau_{jz}(x,y)=b_z\times\begin{cases}k^1_{jz}(x,y,\eta,\zeta), & 0\leqslant y\leqslant\zeta\\ k^2_{jz}(x,y,\eta,\zeta), & \zeta\leqslant y\leqslant h\end{cases}\quad j=x,y \tag{19}$$

where $k^l_{jz}(x,y,\eta,\zeta)$, $l=1,2$, $j=x,y$ are the coefficients of b_z and may be deduced from (14) and (17) for the two different formulations. It is worth emphasizing that in Eq. (19), wherever the line joining points (x,y)

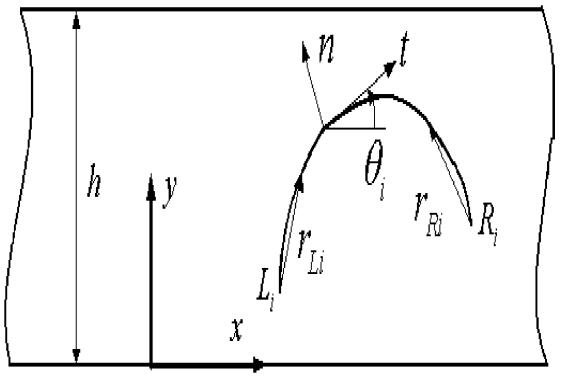

Fig. 2. Schematic view of a curved crack.

and (η,ζ) makes small angle ($\leqslant 1^\circ$) with the center-line of strip the series solution for screw dislocation otherwise the integral form of solution should be invoked.

Let N be the number of cracks in the strip, Fig. 2. The curved crack configuration with respect to coordinate system x, y may be described in parametric form as

$$\begin{aligned} x_i &= \alpha_i(s) \\ y_i &= \beta_i(s), \quad i = 1,2,\ldots,N, \quad -1 \leqslant s \leqslant 1 \end{aligned} \tag{20}$$

The moveable orthogonal t, n coordinate system is chosen such that the origin may move on the crack while t-axis remains tangent to the crack surface. The anti-plane traction on the surface of ith crack in terms of stress components in the cartesian coordinates become

$$\tau_{nz}(x_i,y_i) = \tau_{yz}\cos\theta_i - \tau_{xz}\sin\theta_i \tag{21}$$

where $\theta_i(s) = \tan^{-1}(\beta_i'(s)/\alpha_i'(s))$ is the angle between x and t axes and prime denotes differentiation with respect to the argument. Suppose screw dislocation with unknown densities $B_{zj}(t)$, are distributed on the infinitesimal segment $\sqrt{[\alpha_j'(t)]^2 + [\beta_j'(t)]^2}\,\mathrm{d}t$ at the surface of jth crack where the parameter $-1 \leqslant t \leqslant 1$. The anti-plane traction on the surface of ith crack due to the presence of above-mentioned distribution of dislocations on all N cracks yield

$$\tau_{nz}(\alpha_i(s),\beta_i(s)) = \sum_{j=1}^{N}\int_{-1}^{1} K_{ij}(s,t)\sqrt{[\alpha_j'(t)]^2 + [\beta_j'(t)]^2}B_{zj}(t)\,\mathrm{d}t, \quad -1 \leqslant s \leqslant 1, \;\; i = 1,2,\ldots,N \tag{22}$$

where

$$K_{ij}(s,t) = \begin{cases} -k_{xz}^1(\alpha_i,\beta_i,\alpha_j,\beta_j)\sin\theta_i + k_{yz}^1(\alpha_i,\beta_i,\alpha_j,\beta_j)\cos\theta_i, & 0 \leqslant \beta_i \leqslant \beta_j \\ -k_{xz}^2(\alpha_i,\beta_i,\alpha_j,\beta_j)\sin\theta_i + k_{yz}^2(\alpha_i,\beta_i,\alpha_j,\beta_j)\cos\theta_i, & \beta_j \leqslant \beta_i \leqslant h \end{cases} \tag{23}$$

The functions $k_{jz}^l(\alpha_i,\beta_i,\alpha_j,\beta_j)$, $l = 1,2$, $j = x,y$ are introduced in (19), we should point out that in (23) quantities with subscript i are functions of s whereas those with subscript j are functions of t. By virtue of the Buckner's principal (Korsunsky and Hills, 1996), the elasticity problem of a strip in the absence of cracks under external loading should be solved which yields the traction on the crack surfaces with opposite sign. Therefore, the left-hand side of Eq. (22) may be specified. The kernels of Eq. (22) are singular as $r \to 0$, where $r = \sqrt{(\alpha_i(s) - \alpha_j(t))^2 + (\beta_i(s) - \beta_j(t))^2}$. As was discussed previously, the dominant singularity

of stress fields for dislocation as $r \to 0$ is of Cauchy type. Consequently, Eq. (22) are Cauchy singular integral equations for the dislocation densities. Employing the definition of dislocation density function, the equation for the crack opening displacement across the jth crack become

$$w_j^-(s) - w_j^+(s) = \int_{-1}^{s} \sqrt{[\alpha_j'(t)]^2 + [\beta_j'(t)]^2} B_{zj}(t)\,\mathrm{d}t, \quad j = 1, 2, \ldots, N \tag{24}$$

The displacement field is single-valued out of crack surfaces. Thus, the dislocation densities are subjected to the following closure requirement:

$$\int_{-1}^{1} \sqrt{[\alpha_j'(t)]^2 + [\beta_j'(t)]^2} B_{zj}(t)\,\mathrm{d}t = 0, \quad j = 1, 2, \ldots, N \tag{25}$$

To obtain the dislocation density, the integral equations (22) and (25) are to be solved simultaneously. This is accomplished by means of Gauss–Chebyshev quadrature scheme developed in Erdogan et al. (1973). The stress fields exhibit square-root singularity at the crack tips (Erdogan, 1985). Therefore, the dislocation densities are taken as

$$B_{zj}(t) = \frac{g_{zj}(t)}{\sqrt{1-t^2}}, \quad -1 \leqslant t \leqslant 1, \quad j = 1, 2, \ldots, N \tag{26}$$

Substituting (26) into (22) and (25) and discretizing the domain, $-1 \leqslant t \leqslant 1$, the integral equations reduced to the following system of $N \times m$ linear algebraic equations

$$\begin{bmatrix} A_{11} & A_{12} & \ldots & A_{1N} \\ A_{21} & A_{22} & \ldots & A_{2N} \\ \vdots & \vdots & \ddots & \vdots \\ A_{N1} & A_{N2} & \ldots & A_{NN} \end{bmatrix} \begin{bmatrix} g_{z1}(t_p) \\ g_{z2}(t_p) \\ \vdots \\ g_{zN}(t_p) \end{bmatrix} = \begin{bmatrix} q_1(s_r) \\ q_2(s_r) \\ \vdots \\ q_N(s_r) \end{bmatrix} \tag{27}$$

where the collocation points are

$$\begin{aligned} s_r &= \cos\left(\frac{\pi r}{m}\right), \quad r = 1, 2, \ldots, m-1 \\ t_p &= \cos\left[\frac{\pi(2p-1)}{2m}\right], \quad p = 1, 2, \ldots, m \end{aligned} \tag{28}$$

The components of matrices and vectors in (27) are

$$A_{ij} = \frac{\pi}{m} \begin{bmatrix} K_{ij}(s_1, t_1)\Delta_j(t_1) & K_{ij}(s_1, t_2)\Delta_j(t_2) & \ldots & K_{ij}(s_1, t_m)\Delta_j(t_m) \\ K_{ij}(s_2, t_1)\Delta_j(t_1) & K_{ij}(s_2, t_2)\Delta_j(t_2) & \ldots & K_{ij}(s_2, t_m)\Delta_j(t_m) \\ \vdots & \vdots & \ddots & \vdots \\ K_{ij}(s_{m-1}, t_1)\Delta_j(t_1) & K_{ij}(s_{m-1}, t_2)\Delta_j(t_2) & \ldots & K_{ij}(s_{m-1}, t_m)\Delta_j(t_m) \\ \delta_{ij}\Delta_j(t_1) & \delta_{ij}\Delta_j(t_2) & \ldots & \delta_{ij}\Delta_j(t_m) \end{bmatrix}$$

$$g_{zj}(t_p) = \begin{bmatrix} g_{zj}(t_1) & g_{zj}(t_2) & \cdots & g_{zj}(t_m) \end{bmatrix}^{\mathrm{T}}$$

$$q_j(s_r) = \begin{bmatrix} \tau_{nz}(x_j(s_1), y_j(s_1)) & \tau_{nz}(x_j(s_2), y_j(s_2)) & \cdots & \tau_{nz}(x_j(s_{m-1}), y_j(s_{m-1})) & 0 \end{bmatrix}^{\mathrm{T}} \tag{29}$$

where δ_{ij} in the last row of A_{ij} is the Kronecker delta, superscript T stands for the transpose of a vector and $\Delta_j(t) = \sqrt{[\alpha'_j(t)]^2 + [\beta'_j(t)]^2}$. The stress intensity factors for ith crack in terms of crack opening displacement, Fig. 2, is (Erdogan, 1985)

$$\begin{aligned} (k_{\mathrm{III}})_{\mathrm{L}i} &= \frac{\sqrt{2}}{4}\mu(y_{\mathrm{L}i}) \lim_{r_{\mathrm{L}i}\to 0} \frac{w_i^-(s) - w_i^+(s)}{\sqrt{r_{\mathrm{L}i}}} \\ (k_{\mathrm{III}})_{\mathrm{R}i} &= \frac{\sqrt{2}}{4}\mu(y_{\mathrm{R}i}) \lim_{r_{\mathrm{R}i}\to 0} \frac{w_i^-(s) - w_i^+(s)}{\sqrt{r_{\mathrm{R}i}}} \end{aligned} \tag{30}$$

where the subscripts L and R designate the left and right crack tips, respectively, and the geometry of crack implies

$$\begin{aligned} r_{Li} &= \left[(\alpha_i(s) - \alpha_i(-1))^2 + (\beta_i(s) - \beta_i(-1))^2\right]^{\frac{1}{2}} \\ r_{Ri} &= \left[(\alpha_i(s) - \alpha_i(1))^2 + (\beta_i(s) - \beta_i(1))^2\right]^{\frac{1}{2}} \end{aligned} \tag{31}$$

The substitution of (26) into (24), and the resultant equations into (30) after using the Taylor series expansion of functions $\alpha_i(s)$ and $\beta_i(s)$ in the vicinity of the points $s = \pm 1$ leads to

$$\begin{aligned} (k_{\mathrm{III}})_{\mathrm{L}i} &= \frac{\mu(y_{\mathrm{L}i})}{2}\left[[\alpha'_i(-1)]^2 + [\beta'_i(-1)]^2\right]^{\frac{1}{4}} g_{zi}(-1) \\ (k_{\mathrm{III}})_{\mathrm{R}i} &= -\frac{\mu(y_{\mathrm{R}i})}{2}\left[[\alpha'_i(1)]^2 + [\beta'_i(1)]^2\right]^{\frac{1}{4}} g_{zi}(1) \end{aligned} \tag{32}$$

The solution of Eq. (27) are plugged into (32) to calculate stress intensity factors.

4. Numerical examples

In this section four examples are solved to demonstrate the applicability of the distributed dislocation technique. In these examples all the lengths are normalized by the thickness of strip h, and except for the first example the FGM constant $\lambda = 2$ and the strip is under constant traction $\tau_{yz} = \tau_0$ on the edges. In the first three examples, the quantity for making the stress intensity factors dimensionless is $k_0 = \tau_0\sqrt{L}$ where L is the half length of crack.

4.1. A rotating straight crack

In this example, the effect of FGM exponent λ on the stress intensity factors is studied. The strip is under constant traction on the edges $\tau_{yz} = \tau_0$ and far field traction $\tau_{xz} = \tau_0$ as $|x| \to \infty$. The crack LR with length $2L = 0.5$ is rotating around its center which is fixed on the center-line of strip. The variation of dimensionless stress intensity factors verses the angle of rotation for isotropic strip, i.e., $\lambda = 0$ and FGM strip with $\lambda = 2.0$ and 5.0 are depicted in Fig. 3. At $\theta = \pi/4$ the traction on the crack surface vanishes. Therefore, the stress intensity factors are zero. For isotropic strip, due to the symmetry, the stress intensity factors for crack tips are identical. For FGM strip, using several values of λ, we observed that $|g_z(-1)| > |g_z(1)|$. Thus, as it was expected, the crack opening displacement at the tip with smaller shear modulus is higher

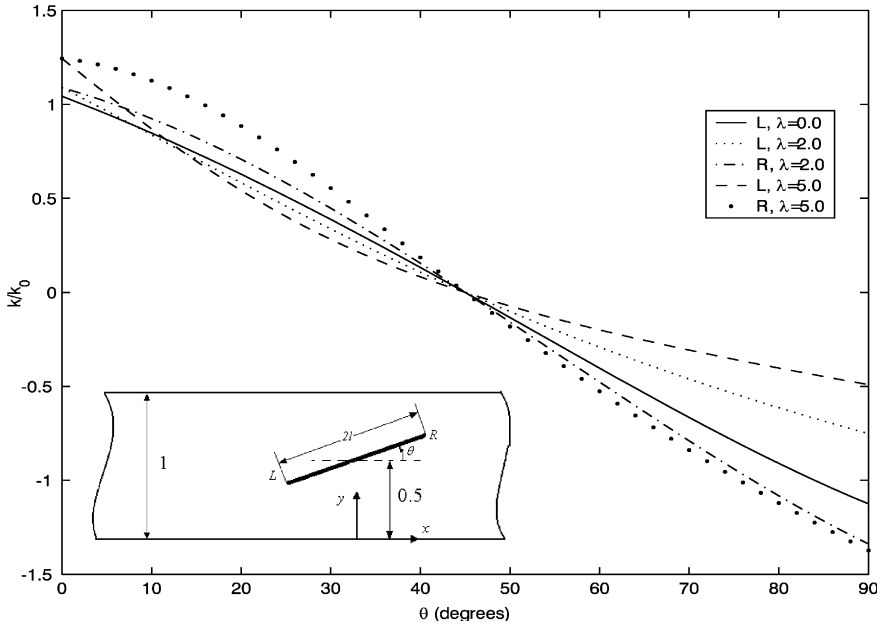

Fig. 3. Dimensionless stress intensity factors for a rotating crack.

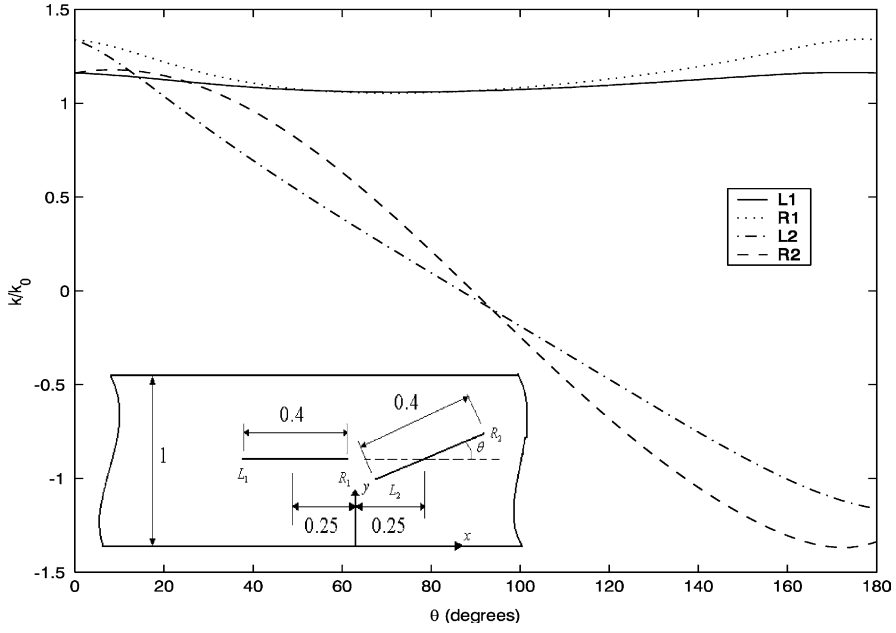

Fig. 4. Dimensionless stress intensity factors for a fixed and a rotating crack.

than the other tip located in higher shear modulus region. However, in Eq. (32), the shear modulus $\mu(y_{Ri}) > \mu(y_{Li})$. The overall effects results in a higher stress intensity factor for the crack tip which is situated in a stiffer zone.

4.2. A fixed and a rotating crack

We consider two equal-length straight cracks situated on the center-line of the strip (Fig. 4). Crack L_1R_1 is fixed while L_2R_2 is rotating around its center. The crack configurations in parametric form are

$$\begin{aligned} x_1 &= -0.25 + Ls \\ y_1 &= 0.5 \\ x_2 &= 0.25 + Ls\cos\theta \\ y_2 &= 0.5 + Ls\sin\theta \quad -1 \leqslant s \leqslant 1 \end{aligned} \tag{33}$$

where $L = 0.2$ is the half length of cracks and θ is the angle between crack L_2R_2 and the x-axis. The variations of k_{L_1} and k_{R_1} are not significant and are due to the change in the interaction between cracks. The value of k_{L_2} at small values of angle θ, $\theta < \pi/12$, is higher than k_{R_2}, which is attributed to the stronger interaction with the fixed crack i.e., distance between L_2 and R_1 is much shorter than between R_2 and R_1. At larger values of angle θ the interaction between the crack tip R_2 and the fixed crack enhances while for L_2 decreases. In addition, the material shear modulus for R_2 is larger than L_2 resulting in $|k_{R_2}| > k_{L_2}|$. At $\theta = \pi/2$ the applied traction on crack L_2R_2 is zero but the interaction between cracks produces unequal values of stress intensity factor at crack tips. The foregoing inequality is valid everywhere, except in a narrow band around $\theta = \pi/2$, which reverses.

4.3. Two parallel off-center cracks

Two off-center equal-length cracks which are parallel to the strip edges are shown in Fig. 5. The centers of cracks remain fixed while the crack lengths are changing with the same rate. The dimensionless stress intensity factors verses crack length are depicted in Fig. 5 for isotropic material and in Fig. 6

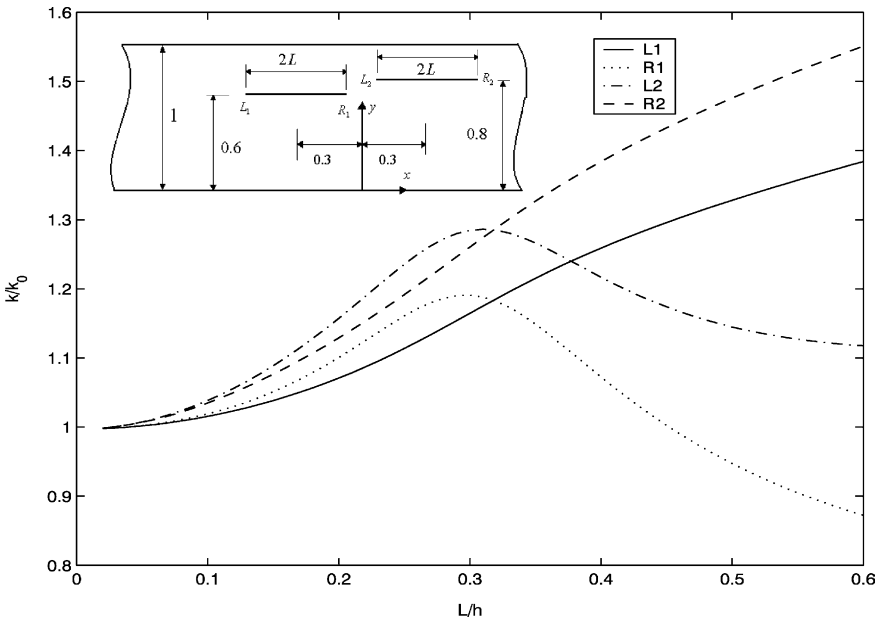

Fig. 5. Dimensionless stress intensity factors for two parallel off-center cracks in an isotropic strip.

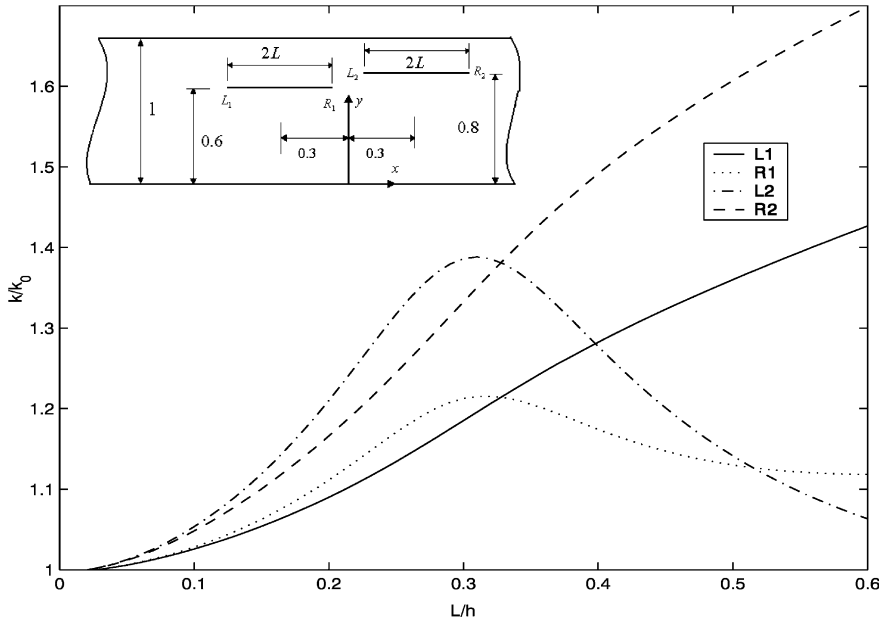

Fig. 6. Dimensionless stress intensity factors for two parallel off-center cracks in a FGM strip.

for FGM. As it might be observed the maximum stress intensity factor for the crack tips R_1 and L_2 occur when the distance between them is minima. For isotropic medium we have $k_{R_2} > k_{L_1}$ and $k_{L_2} > k_{R_1}$, because crack L_1R_1 is closer to the strip center-line. For cracks in FGM the foregoing argument does not hold.

4.4. Two curved cracks

In the last example two curved cracks which are portions of the circumference of an ellipse with the following parametric representations are considered:

$$\begin{aligned} \alpha_i(t) &= x_c + (-1)^i a \cos\left[\frac{1}{2}(1-(-1)^i t)\psi\right] \\ \beta_i(t) &= y_c + b \sin\left[\frac{1}{2}(1-(-1)^i t)\psi\right] \quad -1 \leqslant t \leqslant 1, \quad i = 1,2 \end{aligned} \tag{34}$$

where the angle

$$\psi = \tan^{-1}\left(\frac{a}{b}\cot\varphi\right) \tag{35}$$

and $(x_c, y_c) = (0, 0.3)$ is the coordinates of the center of the ellipse. The lengths of major and minor semi-axes of the ellipse are $a = 0.7$ and $b = 0.5$, respectively. The problem is symmetric with respect to the y-axis. The variation of dimensionless stress intensity factors against angle φ for the crack L_1R_1 are shown in Fig. 7. The normalizing factor in this case is taken as $k_0 = \tau_0\sqrt{a}$. The stress intensity factor k_{R_1} in FGM is higher than k_{R_1} in isotropic material. For the crack tip L_1 the situation reverses. Nonetheless, the variation of stress intensity factor for both materials manifest the same trend.

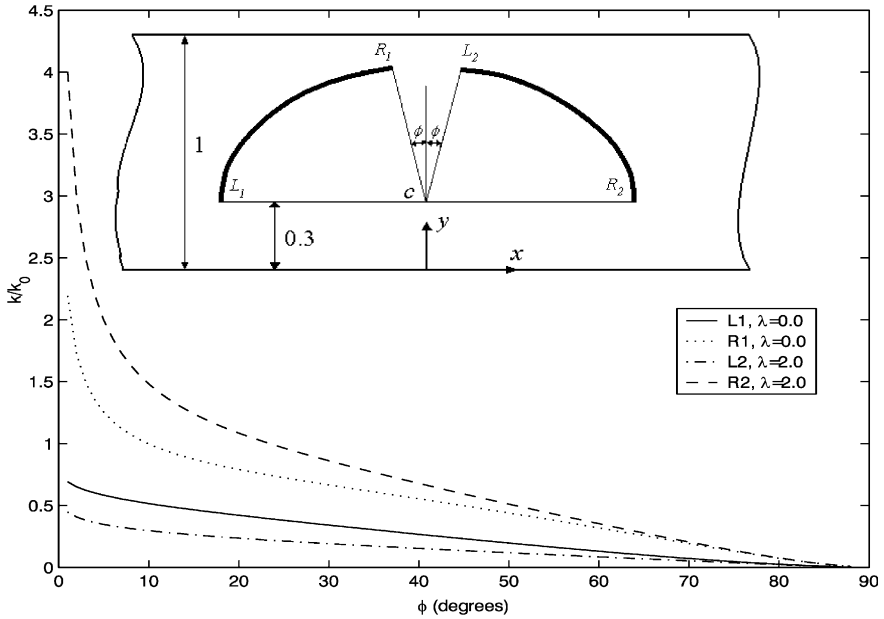

Fig. 7. Dimensionless stress intensity factors for two curved cracks.

5. Conclusion

Stress analysis is carried out in a strip composed of FGM weakened by a screw dislocation. Two solutions are obtained in series and integral forms, which may be considered as the Green's functions for the strip with multiple cracks under anti-plane deformation. The former solution is applicable wherever the line joining dislocation and the point under consideration on the crack surface is almost parallel with the centerline of strip whereas the latter solution converges otherwise. To study the interaction between cracks, and also the effect of crack orientation stress intensity factors are obtained for four examples. Among other findings, we observed that for a straight crack in FGM, stress intensity factors are enhanced as the shear modulus of material increases.

References

Abramowitz, M., Stegun, I.A., 1965. Handbook of Mathematical Functiontions. Dover, New York.

Chan, Y.-S., Paulino, G.H., Fannjiang, A.C., 2001. The crack problem for nonhomogeneous materials under anti-plane shear loading—a displacement based formulation. Int. J. Solids Struct. 38, 2989–3005.

Erdogan, F., 1985. The crack problem for bonded nonhomogeneous materials under antiplane shear loading. Trans. ASME J. Appl. Mech. 52, 823–828.

Erdogan, F., Ozturk, M., 1992. Diffusion problems in bonded nonhomogeneous materials with an interface cut. Int. J. Eng. Sci. 30 (10), 1507–1523.

Erdogan, F., Gupta, G.D., Cook, T.S., 1973. Numerical solution of integral equations. In: Sih, G.C. (Ed.), Methods of Analysis and Solution of Crack Problems. Leyden Holland, Noordhoof.

Erdogan, F., Kaya, A.C., Joseph, P.F., 1991. The mode III crack problem in bonded materials with a nonhomogeneous interfacial zone. Trans. ASME J. Appl. Mech. 58, 419–427.

Faal, R.T., Fotuhi, A.R., Fariborz, S.J., Daghyani, H.R., 2004. Anti-plane stress analysis of an isotropic wedge with multiple cracks. Int. J. Solids Struct. 41, 4535–4590.

Huang, G.-Y., Wang, Y.-S., Gross, D., 2002. Fracture analysis of functionally graded coatings: antiplane deformation. Eur. J. Mech. A—Solids. 21, 391–400.

Korsunsky, A.M., Hills, D.A., 1996. The solution of crack problems by using distributed strain nuclei. Proc. Inst. Mech. Eng. Part C—J. Mech. Eng. Sci. 210 (1), 23–31.

Ozturk, M., Erdogan, F., 1993. Antiplane shear crack problem in bonded materials with a graded interfacial zone. Int. J. Eng. Sci. 31 (12), 1641–1657.

Wang, Y.-S., Huang, G.-Y., Dross, D., 2003a. On the mechanical modeling of functionally graded interfacial zone with a griffith crack: Anti-plane deformation. Trans. ASME J. Appl. Mech. 70, 676–680.

Wang, B.-L., Mai, Y.-W., Sun, Y.-G., 2003b. Anti-plane fracture of a functionally graded material strip. Eur. J. Mech. A—Solids 22, 357–368.